

Tricellulin constitutes a novel barrier at tricellular contacts of epithelial cells

Junichi Ikenouchi,^{1,3} Mikio Furuse,¹ Kyoko Furuse,⁴ Hiroyuki Sasaki,^{4,5} Sachiko Tsukita,^{1,2,3} and Shoichiro Tsukita^{1,3}

¹Department of Cell Biology and ²School of Health Sciences, Faculty of Medicine, Kyoto University, Sakyo-ku, Kyoto 606-8501, Japan

³Solution Oriented Research for Science and Technology, Japan Science and Technology Corporation, Sakyo-ku, Kyoto 606-8501, Japan

⁴Knowledge Action Network Research Institute, Inc., Kyoto Research Park, Chudoji, Shimogyo-ku, Kyoto 600-8317, Japan

⁵Department of Molecular Cell Biology, Institute of DNA Medicine, The Jikei University School of Medicine, Nishi-Shinbashi, Minato-ku, Tokyo 105, Japan

For epithelia to function as barriers, the intercellular space must be sealed. Sealing two adjacent cells at bicellular tight junctions (bTJs) is well described with the discovery of the claudins. Yet, there are still barrier weak points at tricellular contacts, where three cells join together. In this study, we identify tricellulin, the first integral membrane protein that is concentrated at the

vertically oriented TJ strands of tricellular contacts. When tricellulin expression was suppressed with RNA interference, the epithelial barrier was compromised, and tricellular contacts and bTJs were disorganized. These findings indicate the critical function of tricellulin for formation of the epithelial barrier.

Introduction

Tight junctions (TJs) prevent the leakage of solutes through the paracellular pathway of epithelial cells (Tsukita et al., 2001; Matter and Balda, 2003; Anderson et al., 2004; Schneeberger and Lynch, 2004) and are indispensable in establishing the various compositionally distinct fluid compartments within the body of multicellular organisms. Ultrathin section electron microscopy demonstrates that TJs consist of discrete sites of apparent fusion involving the outer leaflet of the plasma membrane of adjacent cells (Farquhar and Palade, 1963). On freeze-fracture electron microscopy, TJs appear as a set of continuous, anastomosing intramembranous particle strands (TJ strands; Staehelin et al., 1969). Each TJ strand associates laterally with another TJ strand in the apposing membranes of adjacent cells to form “paired” TJ strands, where the intercellular space is largely obliterated (Tsukita et al., 2001).

To be more exact, these TJs should be called bicellular TJs (bTJs) between two adjacent cells. At tricellular contacts, where there are three epithelial cells, TJs have been thought to be structurally specialized and are referred to as tricellular TJs (tTJs). The ultrastructure of tTJs has been examined in detail by freeze-fracture replica electron microscopy (Staehelin et al., 1969; Friend and Gilula, 1972; Staehelin, 1973; Wade and Karnovsky, 1974; Walker et al., 1985). As schematically drawn in

Fig. 1, the bTJs are discontinuous at tricellular contacts. As bTJs approach a tricellular contact region, their network extends basolaterally. The central area of these vertically oriented tTJs is composed of three pairs of TJ strands called central sealing elements (Staehelin, 1973), which appear as vertical extensions of the most apical paired strands of the bTJs. At the corner of tricellular contacts, two vertical strands of central sealing elements are associated tightly and laterally within individual plasma membranes, resulting in the formation of a central tube that could be a weak point for the epithelial barrier. From the viewpoint of the epithelial barrier, these two TJ types, bTJs and tTJs, should be considered separately, although the distinction has been largely ignored.

The first constituent of bTJ strands to be identified was occludin (~60 kD; Furuse et al., 1993; Ando-Akatsuka et al., 1996), which consists of four transmembrane domains (Tsukita and Furuse, 1999) and was initially thought to be a major constituent of bTJ strands. However, gene knockout analyses revealed that bTJ strands can be formed and function as barriers in the absence of occludin (Saitou et al., 1998). Using occludin as a probe, a large family of claudins (~23 kD) with 24 family members was subsequently identified as a major constituent of bTJ strands (Furuse et al., 1998a; Morita et al., 1999; Tsukita and Furuse, 1999; Tsukita et al., 2001; Anderson et al., 2004). Claudins also bear four transmembrane domains but do not show any sequence similarity to occludin. Interestingly, when expressed in mouse L fibroblasts, each of the different claudin species polymerized within the plasma membrane to reconstitute paired strands at cell–cell contact regions (Furuse et al.,

Correspondence to Shoichiro Tsukita: htsukita@mfour.med.kyoto-u.ac.jp

Abbreviations used in this paper: bTJ, bicellular TJ; RNAi, RNA interference; SJ, septate junction; TER, transepithelial electric resistance; TJ, tight junction; tTJ, tricellular TJ.

The online version of this article contains supplemental material.

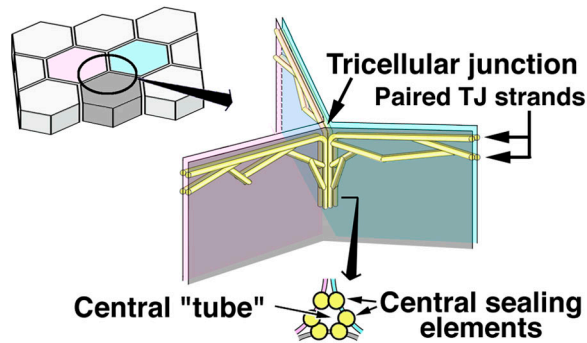


Figure 1. **Schematic drawing of the organization of tTJs.** One tricellular contact (left drawing) is enlarged in the right drawing. See the Introduction for details.

1998b). Claudins and occludin are also found at tTJs, but, to date, no proteins have been identified to be specifically concentrated at tTJs.

TJs completely disappear during epithelial–mesenchymal transition, a process by which epithelial cells lose their polarity (Hay, 1995). Recently, Snail, a transcription repressor, was shown to play a central role in epithelial–mesenchymal transition (Nieto, 2002). In cultured mouse Eph4 epithelial cells expressing Snail (Eph4-mSnail cells), the transcription of claudins and occludin were completely repressed (Ikenouchi et al., 2003). Therefore, we hypothesized that the expression of as yet unidentified bTJ- and tTJ-related integral membrane proteins, if any, might also be suppressed by Snail. We then screened high density oligonucleotide microarrays representing ~24,000 mouse genes for transcripts, whose levels were undetectable in Eph4-mSnail cells compared with parental Eph4 cells (unpublished data), and identified several tetraspan proteins as targets of Snail in addition to claudins and occludin. Interestingly, one of them was uniquely concentrated at tricellular contacts in epithelial cellular sheets, and we named this protein tricellulin. In this study, we show the unique tricellular localization of this protein both at immunofluorescence and electron microscopic levels and clarify its important function in the epithelial barrier through RNA interference (RNAi) analyses.

Results and discussion

Structure and expression of tricellulin

Full-length cDNA encoding tricellulin was isolated from a mouse kidney cDNA library and has an ORF encoding a 555–amino acid polypeptide (63.6 kD) with four predicted transmembrane domains (Fig. S1, available at <http://www.jcb.org/cgi/content/full/jcb.200510043/DC1>). Immunofluorescence staining of cultured cells suggested that both the NH₂ and COOH termini of tricellulin were located in the cytoplasm, as depicted in Fig. 2 A. Interestingly, the COOH-terminal sequence (~130 amino acids) was conserved between tricellulin and occludin; in occludin, this region was reported to be remarkably conserved among various vertebrate species (Ando-Akatsuka et al., 1996) and to contain a domain responsible for its associa-

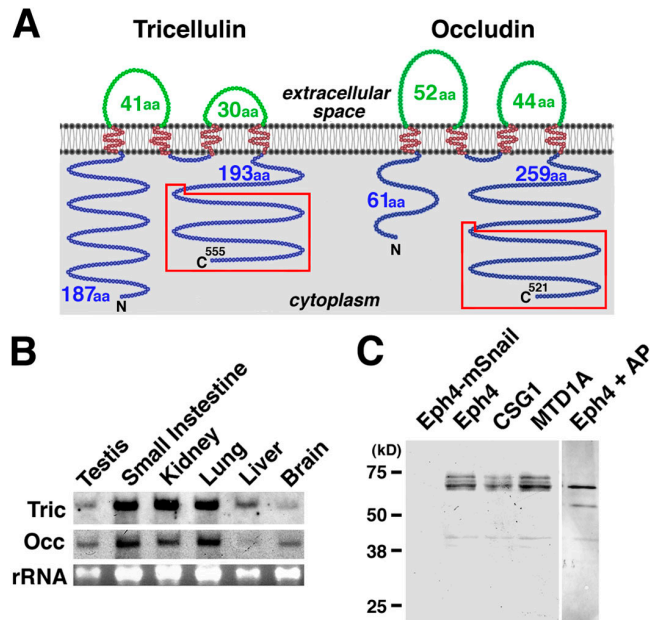


Figure 2. **Structure and expression of mouse tricellulin.** (A) Membrane folding models for mouse tricellulin and occludulin. Tricellulin and occludulin share two structural characteristics in addition to bearing four transmembrane domains: (1) The first extracellular loop has a high content of tyrosine and glycine residues (Fig. S1 B, available at <http://www.jcb.org/cgi/content/full/jcb.200510043/DC1>). (2) The COOH-terminal (C) ~130 amino acids are 32% identical (boxed in red; Fig. S1 C). It should be noted that tricellulin bears a longer NH₂-terminal (N) cytoplasmic domain (187 amino acids) as compared with occludulin (61 amino acids). (B) Northern blotting. Both tricellulin (Tric) and occludulin (Occ) are expressed in large amounts in epithelium-derived tissues. rRNA, ribosomal RNA. (C) Immunoblotting of cultured mouse epithelial cells. The total lysate of Eph4 cells exogenously expressing mouse Snail (Eph4-mSnail; Ikenouchi et al., 2003), Eph4 cells, CSG1 cells, and MTD1A cells were separated by SDS-PAGE followed by immunoblotting with anti-tricellulin pAb. Tricellulin was detected as multiple bands in Eph4, CSG1, and MTD1A cells, but after alkaline phosphatase treatment, there was only a single, smaller Mr band (Eph4 + AP). In Eph4-mSnail cells, tricellulin is undetectable.

tion with ZO-1, a major TJ plaque protein (Furuse et al., 1994). Northern analysis showed that tricellulin mRNA was expressed in large amounts in epithelium-derived tissues (Fig. 2 B). When the whole cell lysate of mouse epithelial cell lines (Eph4, CSG1, and MTD1A) was resolved by electrophoresis and immunoblotted with anti-tricellulin pAb, tricellulin migrated as multiple bands in the Mr range of 66–72 kD, and the band of the lowest Mr was predominant (Fig. 2 C). On alkaline phosphatase treatment of the lysate of Eph4 cells, these multiple bands converged into the lowest Mr band, suggesting that, similar to occludulin (Sakakibara et al., 1997), tricellulin is phosphorylated within cells. Furthermore, it was confirmed also at the protein level that the expression of tricellulin was repressed completely by Snail.

As it has been believed that there is no structurally related protein to occludulin, it was an unexpected finding that tricellulin has some structural similarities to occludulin (Fig. 2 A and Fig. S1). The genes encoding these two proteins are located in tandem on mouse chromosome 13 and human chromosome 5, suggesting that they may have been duplicated during phylogenetic evolution.

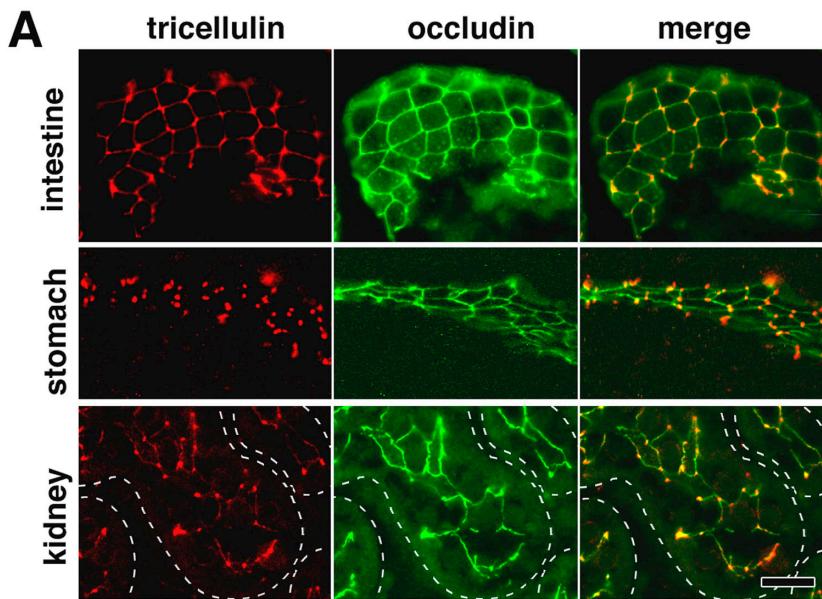
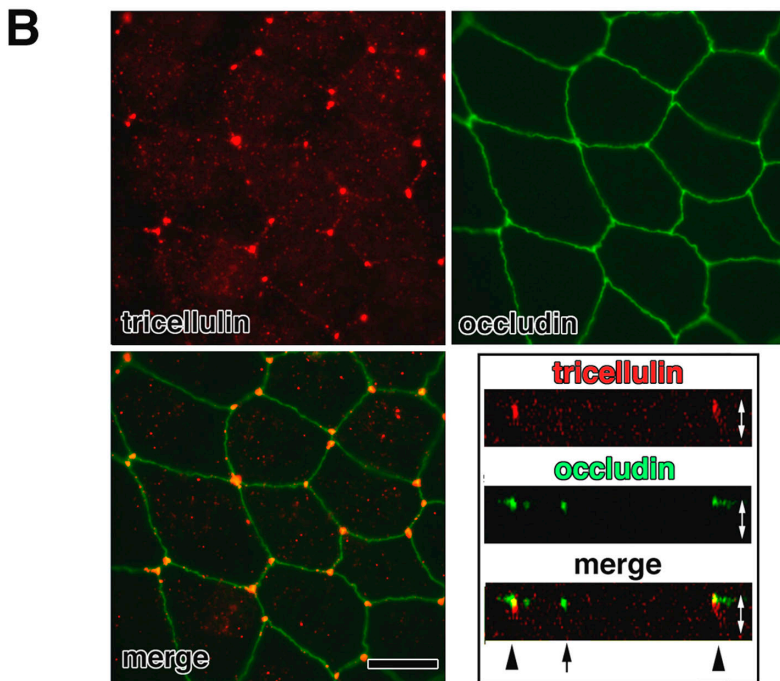


Figure 3. Immunofluorescence localization of tricellulin. (A) Immunofluorescence staining of frozen sections of mouse small intestine, stomach, and kidney doubly with anti-tricellulin pAb (red) and anti-occludin mAb (green). Individual renal tubules in the kidney are represented as dotted lines. Tricellulin was predominantly concentrated at the tricellular contacts, where three occludin-positive bTJs converged. There are also weaker signals at bTJs between two adjacent cells, especially in the small intestine. Bar, 20 μm . (B) Immunostaining of mouse Eph4 cells. Tricellulin (red) was concentrated at each tricellular contact, whereas occludin (green) was distributed along bTJs. The right bottom panel shows vertical sectional images generated from confocal microscopic images. Arrow and arrowheads represent bTJs and tTJs, respectively. White arrows are equivalent in length to the thickness of the cellular sheet. Bar, 10 μm .



Tricellular localization of tricellulin

We then examined the subcellular distribution of tricellulin: immunofluorescently stained frozen sections of epithelial cellular sheets such as the small intestine, stomach, and kidney, doubly with anti-tricellulin pAb and anti-occludin mAb, showed a unique staining pattern (Fig. 3 A) predominantly localized to the tricellular contacts. There are also weaker signals at bTJs between two adjacent cells, especially in the small intestine. When the confluent cellular sheets of the mouse epithelial cell line Eph4 were double stained with anti-tricellulin pAb and anti-occludin mAb, tricellulin was again characteristically concentrated at each tricellular contact as dots where three occludin-positive lines converged (Fig. 3 B). In vertical confocal microscopic

images generated at the tricellular contacts, tricellulin-positive structures appear as vertically oriented short rods, whereas occludin was concentrated as dots only in the most apical region of these rods. A similar tricellular contact-specific concentration of tricellulin was observed in other epithelial cell lines such as mouse MTD1A cells, CSG1 cells, and dog MDCK II cells (Fig. 4 A). To confirm the specificity of the unique staining pattern with anti-tricellulin pAb, we then performed transfection experiments. When HA-tagged tricellulin was exogenously expressed in Eph4 cells followed by double staining with anti-HA pAb and anti-occludin mAb, HA-tagged tricellulin was predominantly recruited to the tricellular contacts, although it was also recruited in small amounts to bTJs (Fig. 4 B).

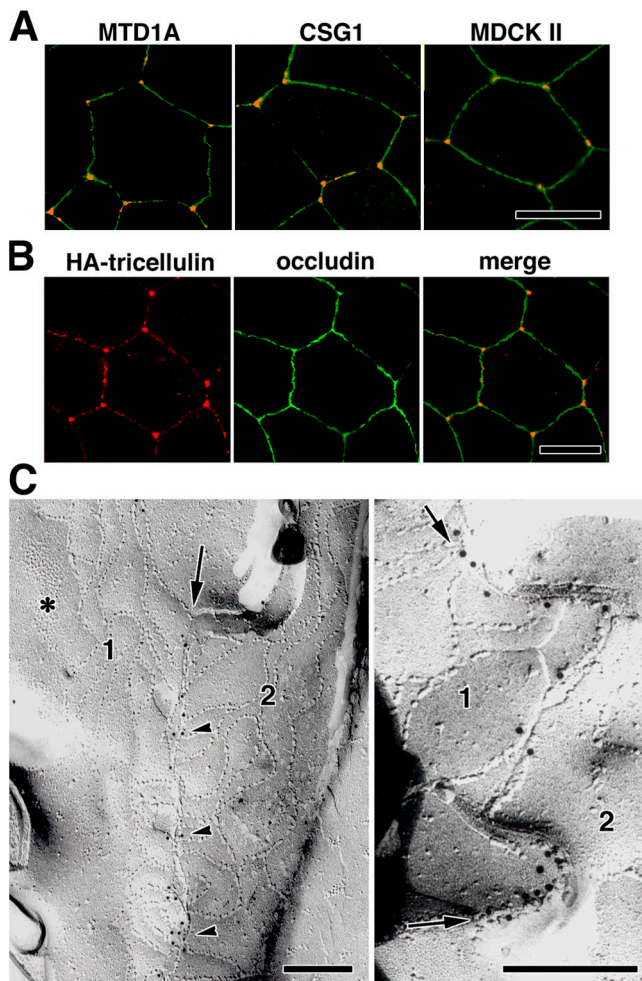


Figure 4. Tricellular localization of tricellulin. (A) Immunostaining of various epithelial cell lines—mouse MTD1A, mouse CSG1, and dog MDCK II cells—with anti-tricellulin pAb (red) and anti-occludin mAb (green). Tricellulin was concentrated at tricellular contacts. (B) Immunostaining of Eph4 cells expressing HA-tagged tricellulin with anti-HA mAb (red) and anti-occludin pAb (green). HA-tricellulin was recruited to the tricellular contacts in large amounts and also to occludin-positive bTJs in small amounts. (A and B) Bars, 10 μ m. (C) Immunofreeze-fracture replica electron microscopy. Freeze-fracture replicas obtained from tricellular contacts of Eph4 cells were immunolabeled with anti-tricellulin pAb. In the left panel, the central sealing elements (arrow), which were identified between bTJ networks of two adjacent cells (1 and 2), were specifically labeled with anti-tricellulin pAb (arrowheads; see Fig. 1). Asterisk indicates adherens junction. In the right panel, the central sealing elements between two adjacent cells (1 and 2) were enlarged, where many immunogold particles were detected (arrows). Bars, 200 nm.

However, the possibility cannot be completely excluded that the tricellular localization of tricellulin is an artifact of image acquisition (e.g., gain settings and antibody affinities). We examined the tricellulin and occludin staining patterns at Eph4 cells with a diluted series of respective antibodies (Fig. S2, available at <http://www.jcb.org/cgi/content/full/jcb.200510043/DC1>). With the diluted antibodies, the tricellular contacts were clearly and specifically marked by anti-tricellulin pAb, whereas occludin did not show any tricellular concentration. Therefore, we conclude that the tricellular localization of tricellulin truly reflects a unique TJ domain.

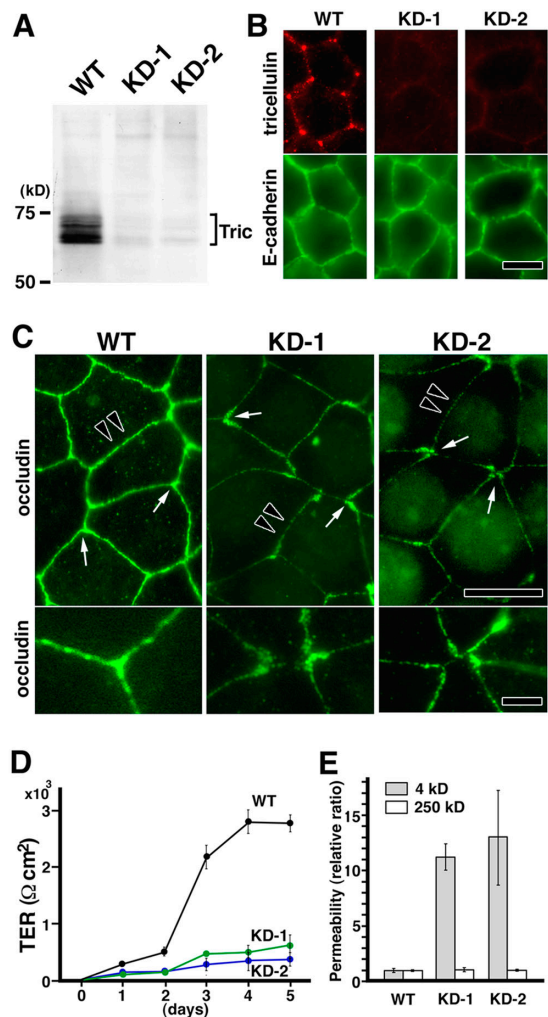


Figure 5. Stable suppression of tricellulin expression in Eph4 cells. (A) Immunoblot analysis using anti-tricellulin pAb. Two independent Eph4 cell clones with suppressed tricellulin expression (KD-1 and KD-2) were established by stably expressing two distinct short interfering RNAs (Brummelkamp et al., 2002). Equal amounts of total proteins were analyzed by SDS-PAGE and immunoblotting. Tric, tricellulin. (B) Immunofluorescence staining of wild-type (WT) and tricellulin RNAi knockdown (KD-1 and KD-2) cells with anti-tricellulin pAb (red) and anti-E-cadherin mAb (green). Bar, 10 μ m. (C) Immunofluorescence staining of WT, KD-1, and KD-2 cells with anti-occludin mAb. In KD-1 and KD-2 cells, both ends of occludin-positive bTJs showed characteristic teardrop-like shapes, and the tricellular contacts were disorganized with gaps (arrows in top panels; enlarged in bottom panels). Furthermore, in these cells, the bTJs were significantly thinner than those in wild-type Eph4 cells (arrowheads in top panels). Bars (top), 10 μ m; (bottom) 3 μ m. (D) TER measurements of WT, KD-1, and KD-2 cells. Tricellulin knockdown significantly affected the development of the epithelial barrier ($n = 10$ for each cell line). (E) FITC-dextran flux measurements of WT, KD-1, and KD-2 cells. There was a significant difference in the flux of 4-kD (but not 250 kD) FITC-dextran across monolayers between wild-type Eph4 cells and KD-1/2 cells ($n = 10$ for each cell line).

The ultrastructure of tTJs is summarized in Fig. 1 (see Introduction). We then examined in which portions of these specialized tTJ structures tricellulin is localized using Eph4 cells by immunofreeze-fracture replica electron microscopy (Fujimoto, 1995). Interestingly, as shown in Fig. 4 C, the central sealing elements were specifically labeled. Taking the intrinsic resolution of immunogold labeling (20–25 nm) into consideration,

most of the immunogold particles appear to label the central sealing elements themselves (Fujimoto, 1995). This labeling pattern was highly consistent with the tricellulin “rods” revealed by confocal microscopy (Fig. 3 B).

As discussed above, tricellulin and occludin may have been duplicated during phylogenetic evolution, but judging from their subcellular localization, they may now have largely nonredundant functions. However, as their distributions in epithelial cells overlapped to some extent, the possibility cannot be excluded that these two related proteins interact with each other in some way to determine and/or modify the structure and functions of TJs. Thus, it is possible that the identification of tricellulin may provide clues as to the function of occludin.

Tricellulin constitutes a novel barrier at tricellular contacts

What happens to the paracellular barrier when the expression of tricellulin is suppressed in epithelial cells? Two independent Eph4 cell clones with suppressed tricellulin expression (KD-1 and KD-2) were established by stably expressing two distinct short interfering RNAs (Brummelkamp et al., 2002). In both clones, tricellulin protein expression was suppressed by >95% as determined by Western blot analysis (Fig. 5 A), and immunofluorescence microscopy did not detect any tricellulin signals at tricellular contacts (Fig. 5 B). Under confluent conditions, KD-1 and KD-2 cells showed a typical cobblestone-like appearance, and there was no significant difference discerned between parental wild-type Eph4 and KD-1/2 cells with regard to the size/shape of individual cells and the distribution of cadherins (Fig. 5 B). However, when KD-1 and KD-2 cells were stained with anti-occludin mAb (Fig. 5 C) or anti-claudin-3 pAb (not depicted), tTJs as well as bTJs showed remarkable structural changes in that both ends of occludin-positive bTJs became thickened into a teardrop shape. At the tricellular contacts, three or more teardrop-shaped ends coalesced, but in most contacts, there remained gaps between these ends. These findings indicated that for a cellular sheet of KD-1/2 cells, the continuity of the TJ network was not maintained in the absence of tricellulin. Furthermore, as shown in Fig. 5 C, in KD-1/2 cells, bTJs themselves appeared to be poorly developed and appeared to be thinner and discontinuous as compared with those in wild-type Eph4 cells. These findings were confirmed by freeze-fracture replica electron microscopy (Fig. S3, available at <http://www.jcb.org/cgi/content/full/jcb.200510043/DC1>). The epithelial barrier function was then compared between wild-type Eph4 and KD-1/2 cells by measuring transepithelial electric resistance (TER; Fig. 5 D) and the flux of membrane-impermeable paracellular tracers (FITC-dextran, 4 and 250 kD; Fig. 5 E). Clearly, when tricellulin was significantly reduced by RNAi, the epithelial barrier was compromised. The TER value did not increase under confluent conditions. Moreover, when challenged with 4 and 250 kD tracers, the paracellular barrier was severely affected in a size-selective manner. These findings have clearly demonstrated that the tricellular contacts play a crucial role in the

epithelial barrier and that tricellulin is directly involved in this novel epithelial barrier mechanism.

The organization of TJs at tricellular contacts has long attracted the interest of cell biologists (Staehelin et al., 1969; Friend and Gilula, 1972; Staehelin, 1973; Wade and Karnovsky, 1974; Walker et al., 1985), as TJs were shown to exhibit a very peculiar structure at each tricellular contact point. However, lack of information concerning the tTJ-specific integral membrane proteins has hampered more direct assessment of the function of tTJs at the molecular level. In the structure depicted in Fig. 1, in the center of tTJs, there is a central tube created by the three paired strands and the three adjoining plasma membranes. Therefore, it is important to know how the leakage of solutes through this tube is prevented and/or regulated. To minimize the diameter of this tube, within individual plasma membranes, two vertical strands of central sealing elements must be laterally associated in a very tight manner. Taking the tricellular contact-specific localization in wild-type Eph4 cells and the disorganization of tTJs in tricellulin knock-down cells into consideration, tricellulin appears to be directly involved in the lateral association of central sealing elements to make TJs functionally continuous at the tricellular contacts and also in the establishment of a barrier at tricellular contacts.

At present, however, it is difficult to attribute the dysfunction of the epithelial barrier induced by suppressing tricellulin expression to the disorganization of only tTJs; immunofluorescence microscopy and freeze-fracture replica electron microscopy showed that tricellulin suppression appeared to affect the organization of not only tTJs but also bTJs (Fig. 5 and Fig. S3). Thus, this dysfunction induced by tricellulin deficiency of the epithelial barrier could not be simply explained by the leakage of solutes through the tricellular corner. It is still premature to further discuss the mechanism for the down-regulation of TER and paracellular tracer transport in KD-1/2 cells. Further detailed analyses are required to answer this issue in the future.

Concluding remarks

Tricellulin is the first protein found to be concentrated at tricellular contacts in vertebrates, but in *Drosophila melanogaster*, gliotactin, a single membrane-spanning protein, was identified at tricellular contacts (Schulte et al., 2003), although these two proteins do not show any sequence similarity. Gliotactin was shown to be involved not only in plugging the tricellular tube but also in establishing the overall organization of bicellular septate junctions (SJs; invertebrate counterparts of TJs). Interestingly, as mentioned above, in tricellulin knock-down cells, the organization of bTJs also appeared to be affected. Thus, it is possible that normal organization of tTJs/SJs is required for the organization and/or stabilization of bTJs/SJs in general.

The identification of tricellulin and its functional analysis are important first steps in expanding the study of the epithelial barrier in vertebrates. Furthermore, tricellulin may represent a novel target for small molecules that modify epithelial tricellular contact points to permit the passage of therapeutic substances to barrier-protected tissues.

Materials and methods

Antibodies and cells

Rabbit anti-GFP pAb and rat anti-HA mAb (3F10) were purchased from Invitrogen and Roche, respectively. Rat anti-occludin mAb (MOC37) was raised and characterized as described previously (Saitou et al., 1998). Rat anti-E-cadherin mAb was provided by M. Takeichi (Center for Developmental Biology, Kobe, Japan).

Rabbit anti-mouse tricellulin (N450) was raised against a GST fusion protein with the NH₂-terminal cytoplasmic domain in rabbits. Rat anti-mouse tricellulin mAbs (N54 and C96) specific for their NH₂- and COOH-terminal cytoplasmic domains, respectively, were generated. Wistar rats were immunized with GST fusion proteins with the NH₂-terminal 150-amino acid or COOH-terminal juxtamembranous 130-amino acid domain, and lymphocytes were fused with P3 myeloma cells to obtain hybridoma cells. All antibodies gave the same results in Western blotting and immunolabeling, but, as one pAb raised against the NH₂-terminal cytoplasmic domain (N450) showed the highest titer among them, we used this pAb in our study.

Epithelial cells (mouse Eph4, CSG1, MTD1A, and dog MDCK cells) were cultured in DME supplemented with 10% FCS.

cDNA cloning, sequencing, and expression vectors

Clone AA759737 was identified as a putative target of Snail in a microarray analysis (probe set ID 106661; MG-U74BV2; Affymetrix, Inc.). A similarity search against the target sequence of clone AA759737 using the Basic Local Alignment Tool programs in the Genome Bioinformatics (University of California, Santa Cruz) identified the mouse EST clone BC003296 (referred to as *Marveld2*). As this EST clone contained only the 3' noncoding and 3' region of the ORF, cDNA encoding the whole ORF was amplified by PCR from a mouse kidney cDNA library (Ikenouchi et al., 2003), and the amplified cDNA was subcloned into the pGEM-T Easy Vector (Promega). To ensure no sequence errors occurred during PCR, the nucleic acid sequence was determined from three independently amplified fragments. The sequence data of cDNA encoding full-length tricellulin/*Marveld2* are available from GenBank/EMBL/DBJ under accession no. AB219935.

To construct a tricellulin expression vector with a HA epitope tag at the COOH terminus, cDNA fragments encoding full-length mouse tricellulin (amino acids 1–555) were produced by PCR and subcloned into the vector pCAGGSneodelEcoRI.

Immunoblotting and alkaline phosphatase treatment

For immunoblotting, proteins were separated by one-dimensional SDS-PAGE and electrophoretically transferred from gels onto nitrocellulose membranes, which were then incubated with the primary antibody. Bound antibodies were detected with biotinylated secondary antibodies and streptavidin-conjugated alkaline phosphatase (GE Healthcare). Nitroblue tetrazolium and bromochloroindolyl phosphate were used as substrates for the detection of alkaline phosphatase. Alkaline phosphatase treatment was performed essentially as described previously (Sakakibara et al., 1997).

Immunolabeling

For immunofluorescence microscopy, cultured cells were fixed with 1% formaldehyde in PBS for 10 min at room temperature, treated with 0.2% Triton X-100 in PBS for 10 min, and washed with PBS. For immunofluorescence microscopy of frozen sections of tissues, dissected samples were frozen in liquid nitrogen, and ~7- μ m-thick sections were cut in a cryostat, mounted on coverslips, air dried, and fixed in 95% ethanol at 4°C for 30 min followed by 100% acetone at room temperature for 1 min. Samples were processed for immunofluorescence microscopy as previously described (Ikenouchi et al., 2003). After being washed with PBS, samples were embedded in 95% glycerol/PBS containing 0.1% p-phenylenediamine and 1% n-propyl gallate and were observed with a fluorescence photomicroscope (Axiophot; Carl Zeiss MicroImaging, Inc.) and a plan Apochromat 63 \times NA 1.40 oil immersion objective (Carl Zeiss MicroImaging, Inc.) with appropriate combinations of filters and mirrors. Photographs were recorded with a cooled CCD camera (model ORCA-ER; Hamamatsu Photonics K.K.) controlled by a Power Macintosh G5 and the software package IPLab V3.9.3 (Scanalytics). Observations were usually at room temperature.

Immunoreplica electron microscopy was performed as described previously (Fujimoto, 1995). Eph4 cells were fixed with 1% PFA in 0.1 M phosphate buffer, pH 7.3, for 5 min at room temperature, washed three times in 0.1 M phosphate buffer, immersed in 30% glycerol in 0.1 M

phosphate buffer for 3 h, and frozen in liquid nitrogen. Frozen samples were fractured at –100°C and platinum shadowed unidirectionally at an angle of 45° in Balzers Freeze Etching System (BAF060; Bal-tec). Samples were immersed and stirred in lysis buffer containing 2.5% SDS, 10 mM Tris-HCl, and 0.6 M sucrose, pH 8.2, for 12 h at room temperature, and then replicas floating off the samples were washed with PBS containing 5% BSA. These replicas were processed for immunolabeling with anti-tricellulin pAb as previously described (Fujimoto, 1995).

Suppression of tricellulin expression

To suppress tricellulin expression levels in Eph4 cells, DNA oligonucleotides of the target sequences encoding two distinct portions of its COOH-terminal tail were cloned into H1 promoter RNAi vector (Brummelkamp et al., 2002). Two distinct RNAi constructs (KD-1 and KD-2) were transfected into Eph4 cells and were effective in suppressing tricellulin expression. Eight clones from each construct were selected.

TER and paracellular tracer flux

Aliquots of 10⁵ cells were plated on Transwell filters 12 mm in diameter (six filters for each cell line), and the culture medium was changed every day. TER was measured directly in culture media using an epithelial voltohmmeter (model Millicell-ERS; Millipore). The TER values were calculated by subtracting the background TER of blank filters and by multiplying by the surface area of the filter.

For paracellular tracer flux assay, after the TER was measured at day 6, 4- or 250-kD FITC-dextran was added to the medium in the apical compartment at a concentration of 1 mg/ml. After a 2-h incubation, an aliquot (100 μ l) of medium was collected from the basal compartment. The paracellular tracer flux was determined as the amount of FITC-dextran in this aliquot of medium, which was measured with a fluorometer.

Online supplemental material

Fig. S1 shows the hydrophilicity plot of the deduced amino acid sequence of mouse tricellulin and the comparison of mouse tricellulin with occludin sequences. Fig. S2 shows the staining pattern of tricellulin and occludin with a diluted series of antibodies. Fig. S3 shows freeze-fracture replica electron microscopy of wild-type Eph4 cells and tricellulin knockdown cells. Online supplemental material is available at <http://www.jcb.org/cgi/content/full/jcb.200510043/DC1>.

We thank all of the members of our laboratory (Department of Cell Biology, Faculty of Medicine, Kyoto University) for helpful discussions.

This study was supported in part by a Grant-in-Aid for Cancer Research and a Grant-in-Aid for Scientific Research (A) from the Ministry of Education, Science, and Culture of Japan to Sh. Tsukita.

Submitted: 7 October 2005

Accepted: 16 November 2005

References

- Anderson, J.M., C.M. Van Itallie, and A.S. Fanning. 2004. Setting up a selective barrier at the apical junction complex. *Curr. Opin. Cell Biol.* 16:140–145.
- Ando-Akatsuka, Y., M. Saitou, T. Hirase, M. Kishi, A. Sakakibara, M. Itoh, S. Yonemura, M. Furuse, and Sh. Tsukita. 1996. Interspecies diversity of the occludin sequence: cDNA cloning of human, mouse, dog, and rat-kangaroo homologues. *J. Cell Biol.* 133:43–47.
- Brummelkamp, T.R., R. Bernards, and R. Agami. 2002. A system for stable expression of short interfering RNAs in mammalian cells. *Science* 296:550–553.
- Farquhar, M.G., and G.E. Palade. 1963. Junctional complexes in various epithelia. *J. Cell Biol.* 17:375–412.
- Friend, D.S., and N.B. Gilula. 1972. Variations in tight and gap junctions in mammalian tissues. *J. Cell Biol.* 53:758–776.
- Fujimoto, K. 1995. Freeze-fracture replica electron microscopy combined with SDS digestion for cytochemical labeling of integral membrane proteins. Application to the immunogold labeling of intercellular junctional complexes. *J. Cell Sci.* 108:3443–3449.
- Furuse, M., T. Hirase, M. Itoh, A. Nagafuchi, S. Yonemura, Sa. Tsukita, and Sh. Tsukita. 1993. Occludin: a novel integral membrane protein localizing at tight junctions. *J. Cell Biol.* 123:1777–1788.
- Furuse, M., M. Itoh, T. Hirase, A. Nagafuchi, S. Yonemura, Sa. Tsukita, and Sh. Tsukita. 1994. Direct association of occludin with ZO-1 and its possible involvement in the localization of occludin at tight junctions. *J. Cell Biol.* 127:1617–1626.

- Furuse, M., K. Fujita, T. Hiragi, K. Fujimoto, and Sh. Tsukita. 1998a. Claudin-1 and -2: Novel integral membrane proteins localizing at tight junctions with no sequence similarity to occludin. *J. Cell Biol.* 141:1539–1550.
- Furuse, M., H. Sasaki, K. Fujimoto, and Sh. Tsukita. 1998b. A single gene product, claudin-1 or -2, reconstitutes tight junction strands and recruits occludin in fibroblasts. *J. Cell Biol.* 143:391–401.
- Hay, E.D. 1995. An overview of epithelio-mesenchymal transformation. *Acta Anat. (Basel)*. 154:8–20.
- Ikenouchi, J., M. Matsuda, M. Furuse, and Sh. Tsukita. 2003. Regulation of tight junctions during epithelial-mesenchymal transition: Direct repression of the gene expression of claudins/occludin by Snail. *J. Cell Sci.* 116:1959–1967.
- Matter, K., and M.S. Balda. 2003. Signalling to and from tight junctions. *Nat. Rev. Mol. Cell Biol.* 4:225–236.
- Morita, K., M. Furuse, K. Fujimoto, and Sh. Tsukita. 1999. Claudin multigene family encoding four-transmembrane domain protein components of tight junction strands. *Proc. Natl. Acad. Sci. USA.* 96:511–516.
- Nieto, M.A. 2002. The snail superfamily of zinc-finger transcription factors. *Nat. Rev. Mol. Cell Biol.* 3:155–166.
- Saitou, M., K. Fujimoto, Y. Doi, M. Itoh, T. Fujimoto, M. Furuse, H. Takano, T. Noda, and Sh. Tsukita. 1998. Occludin-deficient embryonic stem cells can differentiate into polarized epithelial cells bearing tight junctions. *J. Cell Biol.* 141:397–408.
- Sakakibara, A., M. Furuse, M. Saitou, Y. Ando-Akatsuka, and Sh. Tsukita. 1997. Possible involvement of phosphorylation of occludin in tight junction formation. *J. Cell Biol.* 137:1393–1401.
- Schneeberger, E.E., and R.D. Lynch. 2004. The tight junction: a multifunctional complex. *Am. J. Physiol. Cell Physiol.* 286:C1213–C1228.
- Schulte, J., U. Tepass, and V.J. Auld. 2003. Gliotactin, a novel marker of tricellular junctions, is necessary for septate junction development in *Drosophila*. *J. Cell Biol.* 161:991–1000.
- Staehein, L.A. 1973. Further observations of the fine structure of freeze-cleaved tight junctions. *J. Cell Sci.* 13:763–786.
- Staehein, L.A., T.M. Mukherjee, and A.W. Williams. 1969. Freeze-etch appearance of tight junctions in the epithelium of small and large intestine of mice. *Protoplasma.* 67:165–184.
- Tsukita, Sh., and M. Furuse. 1999. Occludin and claudins in tight junction strands: leading or supporting players? *Trends Cell Biol.* 9:268–273.
- Tsukita, Sh., M. Furuse, and M. Itoh. 2001. Multifunctional strands in tight junctions. *Nat. Rev. Mol. Cell Biol.* 2:285–293.
- Wade, J.B., and M.J. Karnovsky. 1974. The structure of the zonula occludens. A single fibril model based on freeze-fracture. *J. Cell Biol.* 60:168–180.
- Walker, D.C., A. MacKenzie, W.C. Hulbert, and J.C. Hogg. 1985. A re-assessment of the tricellular region of epithelial cell tight junctions in trachea of guinea pig. *Acta Anat. (Basel)*. 122:35–38.